Dynamics of Capillary Evaporation. I. Effect of Morphology of Hydrophobic Surfaces

Alenka Luzar[1] and Kevin Leung[2]

[1]Department of Pharmaceutical Chemistry, University of California, San Francisco, CA 94143-0446, and Hilgard Hall-3110, University of California, Berkeley, CA 94720-3110

[2]Sandia National Laboratories, MS 1421, Albuquerque, NM 87185

(June 7, 2000)

Abstract

Capillary evaporation (cavitation) has been suggested to be a possible source of long range interactions between mesoscopic hydrophobic surfaces. While evaporation is predicted by thermodynamics, little is known about its kinetics. Glauber dynamics Monte Carlo simulations of a lattice gas close to liquid-gas coexistence and confined between partially drying surfaces are used to model the effect of water confinement on the dynamics of surface-induced phase transition. Specifically, we examine how kinetics of induced evaporation change as the texture of hydrophobic surfaces is varied. Our results provide guidelines for efficient manipulation of surface properties. We find that evaporation rates can be considerably slowed upon deposition of relatively small amount of hydrophilic coverage. The distribution of hydrophilic patches is however crucial, with the regularly spaced distribution being much more effective in slowing the formation of vapor tubes that trigger the evaporation process. To relate simulation rates to experimental ones, we also perform simulations using the mass-conserving Kawasaki algorithm. We predict evaporation time scales that range from hundreds of picoseconds in the case of mesoscopic surfaces $\sim 10^4$ nm^2 to tens of nanoseconds for smaller surfaces ~ 40 nm^2, when the two surfaces are ~ 10 solvent layers apart. The present study demonstrates that cavitation is kinetically viable in real systems and should be considered in studies of processes at confined geometry.

I. INTRODUCTION

At macroscopic and mesoscopic interfaces hydrogen bonding cannot persist to the extent found in bulk liquid. It has been established by mean-field models,[1,2] computer simulations[3] and surface vibrational spectroscopy[4] that each interfacial water molecule sacrifices one hydrogen bond near extended hydrophobic surfaces. This energy change is larger than the van der Waals attraction with the surface at ambient conditions, where energy of a hydrogen bond is a few k_BT, and a reduction in water density near the surface is expected. An example of such depletion is the hydration of the melittin dimer where the inverted clathrate structure of water was found, characterized by a less favorable water-water binding energy.[5] The loss of hydrogen bonding and associated energetic effect increases the propensity for drying. In the case of water confined between two hydrophobic surfaces, depletion of hydrogen bonds and associated reduced density lead to an anisotropy of the local pressure and possible cavitation, either of which can give rise to an attractive force between the surfaces.[6] Thus, the issues of spontaneous nucleation of a vapor phase (cavity) in water between finite mesoscopic surfaces pertain to problems of adhesion, formation of self-assemblies and also interactions involving proteins.

Water confined between two hydrophobic surfaces in close proximity is replaced by vapor due to competition between bulk energetics (that favors the liquid phase) and surface energetics (that favors the vapor phase). The critical distance, D_c, between ideal hydrophobic surfaces of lateral size L, below which vapor represents the stable phase is:[7]

$$D_c \sim 2\Delta\gamma/(\rho\Delta\mu + b\gamma/L), \tag{1}$$

where Young equation gives $\Delta\gamma \equiv \gamma_{wl} - \gamma_{wv} = -\gamma\cos\theta_c$. γ_{wl}, γ_{wv} and γ denote wall/liquid, wall/vapor and liquid/vapor surface tension, θ_c, is the contact angle, ρ is the number density of water, $\Delta\mu$ is the difference of the chemical potential of bulk liquid from liquid-vapor coexistence, and b is a geometry dependent constant of the order of unity. At ambient conditions for water, $\Delta\mu$ is small, and 100 nm$< D_c <$ 1000 nm. In light of this fact, many theoretical studies suggest that the physics of evaporation and surface drying is pertinent to the interactions between large hydrophobic surfaces separated at mesoscopic scales.[7–14]

Although cavitation or capillary evaporation is favored thermodynamically (Eq.1), large free energy barriers may preclude evaporation over macroscopic times of observation.[15–17] Because of metastability of water present in confined hydrophobic environments,[18–20] special emphasis has to be paid to the dynamical aspects. Understanding the mechanisms by which spontaneous cavitation or bubble nucleation occur in practice require a consideration of activation energies, fluctuations, and kinetics associated with the creation of the various new interfaces during the nucleation process.[21] These pertinent factors are missing in most of the earlier studies.[8–13]

The mechanism and kinetics of evaporation should be amenable to studies by computer simulation techniques. So far, molecular simulations have reproduced the evaporation only at small separations, up to three molecular layers. Recently we have come to understand the origin of this behavior.[7] For specific conditions of the calculations, grand canonical Monte Carlo simulation of the BBL model of water[22] confined between infinite inert plates[23] and constant pressure molecular dynamics of the RER model of water[24] between two ellipsoidal solutes, each with surface ~ 2.5 nm^2,[25] captured spontaneous evaporation at distances

DISCLAIMER

DISCLAIMER

Portions of this document may be illegible in electronic image products. Images are produced from the best available original document.

consistent with Eq. 1. These molecular simulations confirm the pertinent physics at small separations of *large* hydrophobic objects:[11,12,26] water confined to only a few molecular layers vaporizes because the water molecules cannot bond to an adequate number of neighboring water molecules. Since a density profile associated with surface drying[27] may contain a free liquid-vapor interface, the pathway to evaporation may involve interfacial capillary wave fluctuations[28–30] — even though these fluctuations may be quenched by the proximity of the liquid-vapor to the drying surface.[31] Due to the long wavelength nature of these capillary wave-like fluctuations, one must account for a large lateral system size — a problem that cannot be overcome by using periodic boundary conditions.[32]

Lattice gas models[33] provide a conventional framework for computations at large length scales. They can reproduce the dynamics on mesoscopic scales, allowing for the investigation of non-equilibrium behavior over a much broader range of length and time scales than is possible with off-lattice models. Note that at large length scales, evaporation of a fluid confined between two drying walls is mathematically isomorphic to the condensation of a vapor between two wetting walls. In the latter case, the phenomenon is known as "capillary condensation."[34] Extensive discussions on the topic as applied to lattice gas models are abound.[29,35–41] Most of this previous work considers an *equilibrium* aspect of capillary phase transition, i.e., phase behavior and wall-induced shift of the first order liquid-gas type transition in thin film geometry. Our present and previous[7] work focuses on the *dynamical* aspect of the phenomenon. The kinetic pathway of the first order phase transition has been previously elucidated using lattice gas simulations in confined geometry.[7] These simulations gave direct evidence that both long and short wavelength fluctuations are important features in the evaporation process. The early long-wavelength stage, corresponding to the detachment of a liquid from a surface is followed by short wavelength fluctuations, i.e., formation of vapor tubes that bridge across the interfaces. These vapor tubes are essential for the evaporation process.

The pathway to evaporation described above has so for been explained for uniform drying walls.[7] In nature hydrophobic surfaces are *partially* drying, i.e., the surface tension of a hydrophobic surface in air or water vapor is lower than in water, and the contact angle of water on the surface, θ_c, is larger than 90^o. In fact, the contact angle determined for oil/water system by the Young equation is $\sim 124^o$, pointing to $\sim 20\%$ attractive surfaces (relative to completely hydrophilic surfaces). Therefore we should have weakly attractive surfaces to model the dispersive forces, not the non-interacting hard walls used in Ref. 7. Furthermore, virtually all surfaces, and particulary those of applied interest, are chemically heterogoenous. Thus, defects that attract the liquid may exist, pinning the liquid layer at defect sites on the walls and quenching the long wavelength interface fluctuations. Examples would be absorbed ions or defects in the coating layer grafted on to mica cross cylinders in a surface force apparatus which lead to the hydrophilic mica surface being exposed to the liquid. These defects or attractive regions will henceforth be denoted "hydrophilic patches," even though the liquid of interest may not necessarily be water. In all situations in nature hydrophobic and hydrophilic interactions are typically mixed together quite intimately. As such, the size and coverage of hydrophilic patches on hydrophobic surfaces, as well as their placement (random vs regular) is expected to have a strong impact on the evaporation time. Both low hydrophilic coverage—the regime most interesting for materials science, and the higher hydrophilic coverage—the regime of interest for molecular biology—should have an

influence on capillary wave-like fluctuations and the formation of vapor tubes. It would be interesting to compare and contrast the rate limiting step in the evaporation process in both regimes.

The size of hydrophobic surfaces themselves may change the pathway to evaporation kinetics. Previous simulations results[7] indicate that in the case of mesoscopic surfaces, long range fluctuations facilitate cavitation. Molecular simulations[25] indicate that diffusion dynamics is sufficient for water to evaporate from microscopic cavities. So far it is not clear at which size (or degree of hydrophobicity) each mechanism dominates. In biological systems, many proteins have large hydrophobic regions on the surface. A recent survey of hydrophobic patches on the surface of 112 soluble, monomeric proteins shows that a relatively large percentage of protein surface ($\sim 30\%$) is comprised of apolar material.[42] The largest hydrophobic region on an individual protein is approximately around 40 nm^2 but can range from 20 to 120 nm^2.[42] The size of typical hydrophobic regions may not be large enough for cavitation to be driven by interfacial fluctuations as is the case with extended hydrophobic surfaces.[7] However, unfolded or partly folded proteins have much larger exposed hydrophobic areas than the native ones, so they have a stronger tendency to aggregate. The same pronounced hydrophobicity can be responsible for the affinity between a chaperone and unfolded or partly folded protein.[43,44]

We systematically investigate the effect of altering surface texture (i.e., changing degree of hydrophilic coverage and distribution of patches) and area on the kinetics of capillary evaporation.[46] Hydrophilic patches of various size and coverage are included in Glauber dynamics[45] Monte Carlo simulations. The effect on the evaporation rate can be drastic. On heterogeneous surfaces, the tube preferentially forms in rare regions devoid of such patches. This is reminiscent of the physics of "Lifshitz traps"[48] for electronic states in disordered media; we will show that this analogy is valuable in analyzing the problem at hand. We find that a regular array of hydrophilic patches, which contain no large voids, can exhibit tube formation times at least two orders of magnitude longer than those for an ensemble of randomly placed patches. This result may be significant because the compositional heterogeneity of surfaces in biological system can be regularly patterned.[49]

While these results provide relative times scales of evaporation, we need to establish connection with real (physical) time. Glauber dynamics (see also Ref. 7) does not conserve the order parameter (liquid density) and does not truly describe the dynamics of real fluids. In this work, the effect of mass transport is also examined using Kawasaki dynamics,[50] which locally conserves the number of occupied sites. For small inter-surface separations considered in the present work, it is found, contrary to Glauber dynamics, that diffusion can represent the rate determining process for evaporation.

The paper is organized as follows. Section II describes the model. The results of Glauber dynamics are discussed in Sec. III. The results of Kawasaki dynamics are discussed in Sec. IV. In the last Section we discuss implications of our results for future work. In the following paper (Paper II) we explicitly calculate the free energy barriers of tube formation to complement this work.

II. MODEL

The confined liquid is modeled by a three-dimensional lattice-gas on a cubic lattice of size $L \times L \times D$. The nearest neighbor lattice-gas Hamiltonian is given by

$$H = -\epsilon \sum_{<ij>\in \text{bulk}} n_i n_j - \sum_{i \in \text{surface}} \epsilon_i^s n_i - \mu \sum_i n_i, \tag{2}$$

where $n_i = 0, 1$ represents vapor/liquid like sites. The lattice gas parameters, specifically, the nearest neighbor interaction ϵ, the chemical potential μ, and the lattice spacing a, are chosen such that the corresponding lattice gas exhibits high surface tension, close proximity to liquid-vapor coexistence, and high incompressibility. These are the three features that seem most pertinent for a liquid such as water at ambient conditions. At room temperature, T =300K, the surface tension of water $\gamma = 70$ mN/m. The isothermal compressibility, κ_T, at standard density of water ($\rho_m = 1\text{g/cm}^3$ and pressure $P = 1$ atm) is $\rho k_B T \kappa_T = 0.062$. Here ρ denotes the number density. Model parameters that reproduce desired properties are estimated by employing the quasi-chemical (mean field) approximation due to Guggenheim.[51,52] The reduced pressure for one component lattice gas is given by:

$$PV/kT = (z-1)\ln(1-n) - (z/2)\ln\chi_{00}, \tag{3}$$

where V is the volume, z is the lattice coordination number, n is the mean occupancy, and χ_{00} is the number of contacts between empty sites divided by the number of sites. The latter is obtained by solving the following two equations:

$$\begin{aligned} n &= \chi_{10}^2 \exp(\epsilon/kT)/\chi_{00} + \chi_{10}, \\ 1-n &= \chi_{00} + \chi_{10}, \end{aligned} \tag{4}$$

where the subscript 0 corresponds to an empty site and subscript 1 to an occupied site. χ_{10} is the number of contacts between empty and occupied sites divided by the number of all sites. $V = a^3$, and $z = 6$ for a cubic lattice. We also considered a tetrahedral lattice (i.e., ice-like diamond lattice), but found that this particular geometry performed worse than the cubic one in terms of thermodynamics and dynamics. The reason is that tetrahedral lattice has a large area per bond than a cubic lattice. At fixed surface tension, large area means large ϵ, which brings the system too close to critical temperature.[53]

If we adopt the reasonable zero temperature approximation for surface tension, $\gamma \sim \epsilon/2a^2$, the characteristic properties PV/k_BT, $\rho kT\kappa_T$, and γ are reproduced using $\epsilon = 1.2646 k_B T$ and $a = 0.193$ nm. This value of ϵ ensures that the fluid is far below the critical temperature (i.e., $T/T_c = 0.70$)[53] and, in the absence of surface fields, exists in the one-phase, liquid-like region and is above the roughening transition temperature.[54] We determine the mean occupancy, n, for a bulk system (i.e., no drying walls) ~ 0.965 from equilibrium Glauber dynamics simulations. This value indicates the zero temperature approximation to be valid. Chemical potential $\mu = \mu_{\text{coex}} + \Delta\mu$, where chemical potential at coexsistence $\mu_{\text{coex}} = -6\epsilon/2$, and $\Delta\mu \sim \Delta P/\rho$, with $\Delta P \sim 10^5$ Pa, and $\rho = n/a^3$. $\Delta\mu = 1.84247 \times 10^{-4} k_B T$ ensures that the corresponding lattice-gas is at close proximity to liquid-gas coexistence.

As discussed in the Introduction, the surface field ϵ_i^s should be $\sim 20\%$ of the bulk field ϵ, in order to mimic water next to an oily surface. However, such high value of ϵ_i^s slows down the

simulation significantly and limits the phase space than can be studied. Here we use 10% for all i not belonging to a hydrophilic patch to capture a relatively weak but finite surface-liquid attraction and still ensure a reasonable rate of dynamics for the purpose of this simulation. The resulting contact angle θ_c, obtained from the relation $\epsilon_i^s = [(1 + \cos\theta_c)/2]\epsilon = 0.1\epsilon$ is 143^0.

To undertake a systematic study of the effect of hydrophobic area on evaporation dynamics at constant separation between the surfaces, we perform calculations with different sizes of drying walls, $L = 32, 64, 128, 512$, in units of a. The smaller plates mimic the largest hydrophobic patch on individual proteins,[42] while the bigger plates approximate conditions characterized by inequality $L \gg D$ typical for the surface force apparatus environment.[47] To estimate the effect of changing the separation between the surfaces, we perform calculations with $D = 6 - 10, 14$ and 16 at constant $L = 32$ or 64. Recently it has been shown[36,37] that in extreme cases of sizable (patch diameter comparable to wall-wall separation) and strongly hydrophilic patches, stable liquid bridges may persist between patches on oposing walls. These bridges do not occur within parameter range considered in this work.

To explore the effect of changing hydrophilic coverage on evaporation dynamics for the biggest system studied ($512 \times 512 \times 10$), hydrophilic patches are introduced as 1×1, 2×2, 4×4, and 8×8 square objects at various hydrophilic coverages Θ, with all sizes given in units of a. Each patch on each surface is not allowed to overlap with another patch on the same surface. The choice of the sizes of hydrophilic patches mimic absorbed ions ($\sim$ 0.4 nm), and/or single groups like COO^-, NH_3^+, SO_3^- (at least 0.5 nm), that can be found on hydrophobized mica surfaces in a surface force apparatus environment, for example. The smallest patch size, 1×1, is chosen to explore possible depining effects (see Sec. III). The hydrophilic coverage Θ is defined as the fraction of patch-covered surface sites. At fixed coverage, the number of patches is inversely proportional to their area. The patches are placed either in a regular square array or random distributed. In the former case, the center-to-center distance between patches is denoted as l_s. At the sites with patches, $\epsilon_i^s = \epsilon$ instead of 0.1ϵ.

Open boundary conditions in the directions perpendicular to the walls are used. The fluid confined is thus bounded by liquid layer outside the simulation box and is connected to a bulk reservoir with a given temperature T and chemical potential μ. This choice corresponds to boundary conditions such that the drying walls are finite objects immersed in bulk liquid, like in experimental/biological situations. The Metropolis sampling scheme is used in all Monte Carlo runs.[55] An accelerated Monte Carlo scheme[56] has also been attempted. However, at our temperature (far away from the critical temperature) and in our slab-like geometry, it is found that this algorithm does not lead to an appreciable increase in simulation speed.

III. GLAUBER DYNAMICS

A. Quenched random distribution of hydrophilic patches on hydrophobic surfaces

While Kawasaki dynamics should in principle be used to study the dynamics of evaporation, it proves too costly for systems with more than a marginal amount of hydrophilicity at the wall-fluid interface. For a systematic study of the effect of hydrophilicity on the evaporation time, we continue to rely on Glauber dynamics Monte Carlo simulations. Figure

(1a) shows the cross sections of a system with randomly placed patches of area 8×8 at $\Theta = 18\%$ during a typical Glauber dynamics evaporation run at difference times (passes). We start from a configuration where all sites are occupied (liquid-like). Because vapor is thermodynamically stable in the confined region at this separation (Eq. 1), this initial configuration corresponds to metastable liquid. Stable vapor films develop adjacent to the walls within $\sim$ 160 passes. Note that the interface fluctuations in our case are limited by the lateral length scale where no patches occur; in those regions the vapor film is thickest and fluctuations are large. In regions with patches, the liquid layer is pinned to the wall and fluctuations are small. In panel (b), it is seen that the initial vapor tube forms in a two-dimensional region devoid of hydrophilic patches.

Figure 1 also depicts $(x-z)$ cross section of a $512 \times 512 \times 12$ system without hydrophilic patches and that of a $512 \times 512 \times 10$ system with 2% coverage of 1×1 patches near their respective tube formation thresholds. Compared to the case without hydrophilic patches, the 8×8 patch size system shown in panels (a) and (b) exhibits vapor films that are thinner and pinned at the surface sites containing patches. Generally, the pathway of tube formation is similar to the case without patches,[7] but the effect of surface inhomogeneity is clearly present. In the case of essentially totally drying surfaces ($\epsilon_s = 0.01\epsilon$) in the previous work,[7] such a vapor tube developed at typically $\sim$ 18000 passes. In the present case of weakly attractive hydrophobic surfaces ($\epsilon_s = 0.1\epsilon$) at the same separation ($D = 12$) a tube develops at $\sim$ 1500 passes (not shown here). This discrepancy is due to the fact that the lattice gas parameters in Ref. 7 were not chosen carefully enough to represent a liquid at ambient conditions, i.e., $\rho k_B T \kappa_T$ was smaller by almost an order of magnitude from the experimental value for water, and the system was *below* the roughening temperature.[54] For the system with 1×1 patches in panel (d), the patches are so small that a de-pining of a liquid layer at some places (denoted by arrows) can occur.

At this point we discuss the relation between the vapor film seen in our lattice gas simulations at weakly attractive hydrophobic surfaces, and and the case of water molecules at Lennard-Jones walls seen in molecular simulations.[32,57,58] For an oily wall there is a weak attraction between water and hydrocarbon sites, and there is apparently no "vapor-liquid" interface[57,32,58]. For a lattice gas, an interface occurs in the sense that the mean distance between the wall and the closest occupied lattice site is not zero. The simple lattice gas cannot capture the effect of ordering of molecules at the surface. Nevertheless, we believe the effect of *density* fluctuations in water near the partially drying wall should be approximately captured by the lattice gas. Comparison between lattice and continuum representation is of course restricted to averages over characteristic distance imposed by coarse grained lattice representation.

In Fig. 2a, the mean evaporation time is plotted as a function of hydrophilic coverage for different sized, randomly placed patches. The tube formation time for each individual run is determined as the number of passes at which a fixed number of *breaches* (typically 50) has occurred. A *breach* is defined as a column of empty sites that extends vertically and completely from one wall to another at a particular (x, y) coordinate. Beyond this number of breaches, the system invariably proceeds towards evaporation; i.e., the critical nucleus size has been reached. The linear-log plot suggests an exponential long-time regime. However, for $\Theta \sim 0.4$, the vapor phase will cease to be the stable state, at which point the tube formation time no longer corresponds to an evaporation time. We expect the fast rate (interval with

lower slope) be dominated by the time to locally form a vapor film (< 200 passes), while the slow rate (interval with higher slope) be predominantly due to tube-formation. The tube formation time is shorter in both regimes for the 8×8 case than the 4×4 one at the same coverage. In general, the smaller the number of patches the faster the evaporation. One ready explanation is that vapor tube formation takes place most readily in statistically rare large regions (Lifshitz traps) devoid of patches (see Fig. 1b and Sec. III B). Lifshitz traps are first studied for band edge states in semiconductor alloys, where energetics and dynamics is dominated by the states localized in rare, large regions with concentration of one atomic species that deviates from the mean. In our case, such physics also applies, as follows. The probability of finding a void of area A_f, which is $P(A_f) \sim \exp(-\sigma A_f)$, where σ is the surface density of patches. Larger A_f result in larger local vapor film thickness $\bar{l}$. As has been shown qualitatively, the vapor tube preferentially forms in the larger voids. ($\bar{l}$ is strongly correlated with ΔG^*, the free energy cost of forming the critical nucleas which is the rate limiting step for evaporation. This relation will be treated in more detail in Paper II.) The gross tube formation rate is a sum over heterogeneous rates in voids of area A_f weighted by $P(A_f)$, and is dominated by above average A_f. Voids with large A_f become less and less probable as the number of patches increases, whereas the patch size alone plays only a minor role.

The effect of patch size on evaporation time at fixed hydrophilic coverage of 2.5% is illustrated in Fig. 2b. We compare the various evaporation rates with a "mean-field" simulation in which the hydrophilicity is smeared uniformly across the walls. It shows that heterogeneity on the surface increases the evaporation rate. Even in the vapor film formation-dominated regime, it is incorrect to use a mean-field smearing of the hydrophilicity. An apparent reason is the difference in $\bar{l}$ as well as interface fluctuation amplitude δl for the same hydrophilic coverage but different morphology. In Table I, the effect of changing surface morphology on $\bar{l}$ is tabulated for regularly spaced patches. (A regular distribution is used because the resulting $\bar{l}$ is much easier to analyze.) In rows 2 and 3 of Table I, the coverage is the same, but $\bar{l}$ is substantially different.

When the surface is covered with hydrophilic patches, the liquid film tends to remain pinned at patch site. A typical wavelength is therefore reduced from $O(L)$ to $O(\bar{d})$, where $\bar{d}$ is the average distance between the borders of adjacent patches. This suggests that tube formation times observed for different coverages and patch sizes should depend on a single parameter, $\bar{d}$. In Fig. 3, we present the tube formation times for a variety of different patch sizes and different coverages given in Figs. 2a and 2b, plotted as a function of $\bar{d}$. They appear to fall on a single curve. At small $\bar{d}$ or large σ, the Lifshitz trap argument[48] suggests that ΔG^* is a function of σ, where $\sigma \sim \bar{d}^{-2}$ if we neglect excluded volume effect. In turn, the tube formation time is proportional to $\exp(\Delta G^*/k_B T)$. The data is too sparse in this region to elucidate the exact dependence.

Comparing the results of Figs. 2a and 2b, we see that patches of 8 × 8 area have the same effect on the evaporation time at a coverage of ∼ 15% as do patches of 2 × 2 area at only 2.5% coverage, but almost the same mean patch/patch separation. This observation provides a guideline for preparation of surfaces which facilitate phase transition or slow it down. Very small change in surface composition (small hydrophilic coverage) can hinder evaporation significantly, because at this regime the distance between borders of patches rather than the coverage itself determines the kinetics.

This patch size effect on the evaporation time becomes particularly important when the number density of patches is not low. Figure 2c illustrates the rate dependence on the patch size at constant number of patches on the surfaces. Here, the increase in the size of the patch drastically increases the evaporation time when σ is sufficiently large. Assuming the same random distribution of patches (ignoring excluded volume effect), larger patches give smaller voids than smaller ones. This explains the increase in the tube formation times when going from 2×2 vs 4×4 patch size at the higher σ. An additional, weaker effect present at both values of σ is due to de-pinning (Fig. 1d). The same de-pinning effect also explains the deviation of left most point in Fig. 3 from the general trend for randomly patched surfaces. This particular point corresponds to an extremely small patch size, 1×1.

B. Regular distribution of hydrophilic patches on hydrophobic surfaces

Figure 4 compares the tube formation times for regularly spaced vs. randomly placed patches at various coverages and for different areas of patches. Tube formation is up to two orders of magnitude faster in the latter case. These results show the efficiency of the physics of Lifshitz traps aiding the tube formation. For randomly distributed patches, a finite fraction of voids of above average size is always present on the surface. As larger areas A_f result in bigger vapor film thickness, $\bar{l}$, the tube is most likely to form at biggest voids in the system. Hence, the evaporation rate corresponds to a void size exceeding average A_f. With regular patch distribution on the other hand, the rate is limited to that determined by the average void size which is necessarily below the rate observed at random patch distribution.

For comparison with the case of randomly placed patches, results for regular patch distribution (fixed value of $\bar{d}$) are also included in Fig. 3. While both sets of data reveal a similar dependence of $\bar{d}$, the tube formation times corresponding to random distribution are in general shorter because domains with above-average $\bar{d}$ contribute disproportionately to the overall rate. At small $\bar{d}$, where the data is sparse, we expect the dependence of ΔG^* on $\bar{d}$ to begin to be very different in the cases of regularly spaced and randomly distributed patches. This is because the latter should demonstrate a scaling governed by Lifshitz trap behavior for disordered media while the former does not.

IV. KAWASAKI DYNAMICS

While qualitatively informative, the Glauber dynamics Monte Carlo does not give a physical time/energy scale for the evaporation event. This is because mass transport is accomplished by using non-physical moves. To incorporate the effect of mass transport, we apply an algorithm that combines Kawasaki and Glauber dynamics, as follows. A site and one of its six neighboring sites are selected at random. If one site is occupied and the other is not, an additional removal of a lattice gas is attempted using a Metropolis acceptance criterion. Alternatively, if the neighboring site is outside the simulation box and not inside the walls, we attempt to add/remove a lattice gas in the initial site using Glauber dynamics acceptance rules. This simulates the diffusion of molecules into or from the wall-confined region and is the only non-mass conserving part of the algorithm.

Kawasaki dynamics is extremely slow. If one starts the simulation with all sites occupied, tens of thousands of passes are needed to create a vapor film. Such a time scale is physically uninteresting. In experimental studies, we expect hydrophobic surfaces to have a vapor films already equilibrated on each before the surfaces are brought together. Motivated by this assumption, we start the simulation as follows. We use Glauber dynamics with a "no breach" constraint throughout the simulation box to equilibrate the two interfaces and to ensure vapor tubes do not form prematurely. Here by "equilibrate," we determine the number of passes needed for the total number of occupied sites in the system to reach a plateau value, which is typically ~ 400 passes. Then the "no breach" constraint is released and Kawasaki dynamics is applied at that point. Next, Glauber tube formation time, *without* constraints, is also sampled using the same starting configuration as the Kawasaki run. This three-step process is then repeated to collect statistics.

The comparison of Glauber and Kawasaki tube formation times are shown in Tables II and III for a variety of L, D, and Θ. The Kawasaki dynamics tube formation time τ_K is 50-500 times slower than the Glauber dynamics time τ_G. Calibrating the Kawasaki time step by comparing the self-diffusion constant in water and in our Kawasaki simulations, we provide rough estimates of tube formation times in nanoseconds in these Tables. Since tube formation is activated, taking the ratio τ_K/τ_G should cancel the exponential dependence on ΔG^*. If prefactors due to the two dynamics are weakly dependent on D and Θ, the ratio should be a constant. We find that this ratio converges to ~ 200 for large ($> 10^3$) τ_G (the bracketed number in Tables II and III). The dynamics of interface fluctuations in phase-separating systems is generally complex.[60,61] In our case, it is further complicated by the fact that the tube size can be too small to allow a continuum analysis. Furthermore, we have not pushed the simulations sufficiently far into the asymptotic regions of large τ_G or τ_K. Therefore the τ_K/τ_G ratio is not well understood at this point, and we defer its study to future studies.

After a vapor tube of critical size is formed, the approach towards complete evaporation is also strongly affected by the choice of dynamics. With Glauber dynamics, the time required is 1000-3000 passes for $L = 512, D = 10$. Therefore, with moderate Θ (the cross-over can be determined from Figs. 2 and 3 for different patch sizes), tube formation is already the rate-determining step in the evaporation. With Kawasaki dynamics, we estimate the corresponding cross-over time to be $O(10^6)$. In all the $L = 512$ systems we have looked at, this post nucleation diffusion time τ_d is larger than the tube-formation time. Note, however, that in real systems, hydrodynamic flow plays a major role in post transient dynamics. The former cannot be captured by Kawasaki dynamics that includes diffusion but excludes collective motion.[62] If $\tau_{\text{tube}} < \tau_d$, multiple vapor tubes will form, which prevents τ_d from being estimated with diffusion equation approaches.[60,63] However, τ_d should be diffusion-limited; it does not involve an energy barrier or should not grow exponentially with D or Θ. In contrast, the tube formation time does grow at least exponentially with these parameters. Assuming τ_d depends weakly on D, and using the trends of ΔG^* variation with D for $L = 64$ (see Paper II), we estimate that, for $L = 512$ and $\Theta = 0$, a cross-over to tube formation rate-limiting evaporation occurs at $D \sim 12 - 13$.

V. CONCLUDING REMARKS

Our numerical results illustrate that the dynamics of evaporation of a metastable liquid film confined between partially drying surfaces sprinkled with hydrophilic patches is rather intricate. The evaporation kinetics depend on hydrophilic coverage and patch size, as well as their ordering; the vapor tube formation time increases with increasing hydrophilic coverage, patch size, and the regularity of their placement, due to a combination of Lifshitz trap physics and the effect of the patches on local interface fluctuation amplitudes. Although these results may seem not so surprising from a physics standpoint, the present study is, to the best of our knowledge, the first that quantitatively and systematically examines the effect of chemical inhomogeneity on evaporation rates.

The crucial point we are making is that, while we are aware that these simulations cannot be deemed to treat real water at real hydrophobic surfaces in *molecular details*, we believe that they capture the basic physics that determines the dynamics of cavitation of water between such surfaces. The particular effect of confinement should not be specific only to water. However, it proves to have far reaching consequences particularly for water. Surface drying/wetting, capillary wave-like fluctuations, tube formation dynamics, and longer range cavitation interaction, are important physics that need to be addressed in "confined" water problems.

A review of experimental work to date[47] on confinement effects of different hydrophobic surfaces in water points to the importance of morphology and structure of hydrophobic surfaces, and how their properties may change during the interaction of two surfaces. Our calculations explicitly address these important situations. For materials scientists they can provide guidelines on how to prevent adhesion with little change in surface composition. In order to drastically reduce the rate of water evaporating from confining surfaces, a very low hydrophilic coverage is sufficient provided the patches are small and evenly distributed.

On the other end, surface induced metastability and cavitation can accompany the folding or assembly of solvated polymers. For biophysicists these qualitative calculations can help in answering questions about which proteins will aggregate faster and why they do so. Let us take two proteins that have the same surface composition on the average but one of them has several small patches and the other has few large ones of either character. The present calculations show that it is the second scenario that will result in faster association. In our future studies the examination of several classes of protein motifs will be carried out in order to more quantitatively determine the extent to which confined water and its surface-induced phase transition plays a role in molecular biology. Biomolecules possessing flat hydrophobic surfaces of larger sizes, e.g., the hydrophobic surfaces of chaperones[64,65] are of our particular interest in order to probe this aspect more thoroughly.

To relate simulation times with real time, we have also performed limited Kawasaki dynamics studies. The longer Kawasaki tube formation times seemingly converges ~ 200 times those of Glauber dynamics runs for a variety of surface sizes and hydrophilic coverages. After calibrating Kawasaki pass with diffusion constant of water, we provide rough approximations for evaporation times. We find time scales of the $O(100)$ps in the case of mesoscopic surfaces $\sim 100 \times 100$ nm^2, and $O(10)$ns for smaller surfaces, $\sim 6 \times 6$ nm^2, with water being confined between partially drying surfaces ~ 2 nm apart in both cases. To relate to the time and length scales accessible to experiments require that a larger interplate

separation be considered.[47] This can be done by combining Kawasaki dynamics results with estimates of free energy barrier for tube formation, to be discussed in more detail in paper II.

ACKNOWLEDGEMENT

We thank D. Bratko, G. S. Grest, J. Israelachvili, S. Marčelja, J. Teixeira, F. van Swol and J. D. Weeks for helpful discussions, and H. Christenson for preprint of Ref. 47. A. L. is grateful for the support from the National Science Foundation (CHE-9806058) and Department of Defense through its High Performance Computing Modernization Program. The work performed at Sandia National Laboratories was supported by the Department of Energy under Contract DE-AC04-94AL85000. Sandia is a multiprogram laboratory operated by Sandia Corporation, a Lockheed Martin Company, for the U.S. Department of Energy.

[1] S. Marčelja, D. J. Mitchell and B. W. Ninham, J. Chem. Soc. Faraday Trans. II **73**, 630 (1977).
[2] A. Luzar et al, Chem. Phys. Lett.96, 485 (1983); *ibid.* J. Chem. Phys. **82**, 5146 (1985).
[3] C. J. Lee, J. A. McCammon, and P. J.Rossky, J. Chem. Phys.**80**, 4448 (1984).
[4] Q. Du, E. Freysz, and Y. R. Shen, Science **264**, 826 (1994).
[5] Y. K. Cheng and P. J. Rossky, Nature 392, 696 (1998).
[6] J. N. Israelachvili, *Intermolecular and Surface Forces*, Academic Press, San Diego, 1991.
[7] K. Lum and A. Luzar, Phys. Rev. E **56**, 6283 (1997).
[8] D. R. Berard, P. Attard, and G. N. Patey, J. Chem. Phys. **89**, 7236 (1993); G. N. Patey, Ber. Busenges. Phys. Chem. **100**, 885 (1996).
[9] V. V. Yaminski and B. W. Ninham, Langmuir **9**, 3619 (1993).
[10] G. Gompper, M. Hauser and A. A. Kornyshev, J. Chem. Phys. **101**, 3378 (1994).
[11] A. Luzar, Faraday Discuss. **103**, 205 (1996).
[12] B. J. Berne, Proc. Nat. Acad. Sci. **93**, 8800 (1996).
[13] K. Lum, D. Chandler and J. Weeks, J. Phys. Chem. B **103**, 4570 (1999).
[14] for a recent review see: J. Teixeira and A. Luzar, *Hydration Processes in Biology*, Les Houches, May 1998, NATO Science Series A **103**, 35 (Washington DC, 1999).
[15] V. S. Yuschencko, V. V. Yaminski and E. D. Shchukin, J. Colloid. Interface Sci. **96**, 307 (1983).
[16] F. Restagno, L. Bocquet and T. Biben, Phys. Rev. Lett. **84**, 2433 (2000).
[17] F. Restagno, L. Bocquet, T. Biben and E. Charlaix, J. Phys. Condens. Matter **12**, A419 (2000).
[18] The experimentally observed hysteresis in the force curve indicates that the hydrophobic interaction may not pertain to equilibrium.
[19] H. K. Christenson and P. M. Claesson, Science **239**, 390 (1988).
[20] J. L. Parker, P. M. Claesson, and P. Attard, J. Phys. Chem. **98**, 8468 (1994).
[21] W. A. Ducker, Z. G. Wu and J. N Israelachvili, Langmuir **10**, 3279 (1994).
[22] D. Bratko, L. Blum and A. Luzar, J. Chem. Phys. **83**, 6367 (1985).
[23] A. Luzar, D. Bratko and L. Blum, J. Chem. Phys. **86**, 2955 (1987).
[24] A. Wallqvist and B. J. Berne, J. Phys. Chem. **51**, 13841 (1993).
[25] A. Wallqvist and B. J. Berne, J. Phys. Chem. **99**, 2893 (1995).
[26] G. Hummer and S. Garde, Phys. Rev. Lett. **80**, 4193 (1998).
[27] F. H. Stillinger, J. Solution Chem. **2**, 141 (1973).
[28] R. Evans, J. Phys. Conden. Matter **2**, 8989 (1990).
[29] A. O. Parry and R. Evans, Physica A **181**, 250 (1992).
[30] J. R. Henderson, Heterogeneous Chemistry Reviews **2**, 233 (1995).
[31] A. Werner, F. Schmid, M. Müller, and K. Binder, J. Chem. Phys. **107**, 8175 (1997).
[32] J. C. Shelley and G. N. Patey, Mol. Phys. **88**, 385 (1996).
[33] K. Binder, A. M. Ferrenberg and D. P. Landau, Ber. Bunsengers. Phys. Chem. **98**, 304 (1994).
[34] K. Binder, Ann. Rev. Phys. Chem. **43**, 33 (1992).
[35] M. Schoen and H. Bock, J. Phys. Condens. Matter **12**, A333 (2000).
[36] P. Rocken and P. Tarazona, J. Chem. Phys. **105**, 2034 (1996).
[37] H. Bock and M. Schoen, Phys. Reve. E **59**, 4122 (1999).

[38] K. Stepniak, A. Patrykiejev, Z. Sokolwska and S. Sokolwski, J. Colloid Interface Sci. **214**, 91 (1999).
[39] A. Huerto, O. Pizio and S. Sokolowski, J. Chem. Phys. **112**, 4286 (2000).
[40] A. Patrykiejev, O. Pizio and S. Sokolowski, Phys. Rev. Lett. **83**, 3442 (1999).
[41] P. Rocken, A. Somoza, P. Tarazona and G. Findenegg, J. Chem. Phys. **108**, 8689 (1998).
[42] P. Lijnzaad, H. J. Berendsen and P. Argos, Proteins **25**, 389 (1996).
[43] E. A. Criag, Science **260**, 1902 (1993).
[44] D. A. Agard, Science **260**, 1903 (1993).
[45] R. Glauber, J. Math. Phys. **4**, 294 (1963).
[46] Note that there is good experimental evidence that ease of cavitation varies between differently prepared Langmuir-Bloodget films, where for example the density and type of hydrophilic patches may vary.[47]
[47] For the latest review on direct measurements of the forces between hydrophobic surfaces in water see H. K. Christenson and P. M. Claesson, Adv. Colloid Interface Sci., preprint.
[48] I.M. Lifshitz, Sov. Phys. Usp. **7**, 549 (1965) [Usp. Fiz. Nauk **83**, 617 (1964)]; R. Friedberg and J. M. Luttinger, Phys. Rev. B. **12**, 4460 (1975).
[49] L. J. Douglas Frink and F. Van Swol, J. Chem. Phys. **108**, 5588 (1998).
[50] K. Kawasaki, Phys. Rev. **145**, 224 (1966).
[51] E. A. Guggenhein, Mixtures, Oxford University Press, Oxford (1952); Proc. R. Soc. London, Sec.A **183**, 213 (1994).
[52] P. Pendzig, W. Dieterich and A. Nitzan, J. Chem. Phys. **106**, 3703 (1997).
[53] The three-dimensional lattice-gas on a simple cubic lattice has a critical point at $k_B T_c/\epsilon = 1.128$ (A. J. Liu and M. E. Fisher, Physica A **165**, 35 (1989).
[54] The interface between the low-density and the high-density phases in lattice-gas model (i. e. discreteness of lattice) undergoes a roughening transition at temperature T_R. This roughening transition is not relevant for liquid-vapor interfaces in real liquids. K. K. Mon, D. P. Landau and D. Stauffer, Phys. Rev. B **42**, 545 (1990) estimated $\epsilon/k_B T_R = 1.636$.
[55] N. Metropolis, A. W. Rosenbluth, M. N. Rosenbluth, A. H. Teller, and E. Teller, J. Chem. Phys. **21**, 1087 (1953).
[56] A. B. Bortz, M. H. Kalos, and J. L. Lebowitz, J. Comp. Phys. **17**, 10 (1975).
[57] C. .Y. Lee, J. A. McCammon and P. J .Rossky, J. Chem. Phys. **80**, 4448 (1984).
[58] D. Bratko et al, to be published.
[59] M. Hasenbusch and S. Meyer, Phys. Rev. Lett. **66**, 530 (1991).
[60] L. A. Turski and J. S. Langer, Phys. Rev. A **22**, 2189 (1977).
[61] K. Kawasaki and T. Ohta, Physica **118A**, 175 (1983).
[62] Hydrodynamic lattice gas calculations in three-dimensions in inhomogeneous systems pose a problem as it is hard to make up a lattice that is "isotropic" in the hydrodynamics sense; for a review, see D. H. Robinson and S. Zaleski, Rev. Mod. Phys. **66**, 1412 (1994).
[63] K. Kawasaki and Y. Enomoto, Physica **135A**, 426 (1986).
[64] K. Z. Braig et al, Nature (London) **371**, 578 (1994);
[65] W. A. Houry et al, Nature (London) **402**, 147 (1999).

FIGURES

FIG. 1. Typical simulation runs that lead to formation of vapor tube in the presence of randomly placed hydrophilic patches (triangles). $L = 512, D = 10$, with $\Theta = 0.18$ coverage of 8×8 patches. (a) Side view of cross sections in the $x-z$ plane as functions of number of Glauber passes. Cells are black when occupied (liquid), and white when empty (vapor). A vapor tube has formed at $t = 1080$. (b) The vapor tube at in the $x-y$ plane (top view) corresponds to $t = 1120$. The crosses and pluses indicate the location of patches on the upper and lower walls, respectively, while the squares depict high vapor density regions. A filled square means zero lattice gas in a given column at coordinate (x, y) (i.e., a "breach" has formed); the open squares of decreasing size indicate one, two, and three lattice gas in that column, respectively. Note that a vapor tube is located in the area free of hydrophilic patches. (c) and (d): $x - z$ cross-sections for $512 \times 512 \times 12, \Theta = 0$ at $t = 1360$, and $512 \times 512 \times 10, 1 \times 1$ patch size, $\Theta = 2\%$ at $t = 1160$, respectively. These snapshots are taken just prior to tube formation. Note the depining of the liquid-vapor interfaces from the hydrophilic patches in panel (d).

FIG. 2. Mean evaporation times (the dashed lines are guides to the eye): (a) As function of hydrophilic coverage, Θ, for 4×4 and 8×8 patches. (b) As function of hydrophilic patch size at constant hydrophilic coverage, $\Theta = 2.5\%$. The first point on the graph (denoting by arrow) corresponds to the uniform smearing of hydrophilicity to all sites adjacent to the walls. (c) As function of hydrophilic patch size at constant surface density, σ. In all cases $L = 512$, $D = 10$.

FIG. 3. Natural logarithm of the mean evaporation time for a variety of patch sizes, and coverages. as a function of the average distance between borders of patches, $\bar{d}$, for randomly placed patches (circles), and for regularly placed patches (triangles). The lines are guides to the eye drawn by considering the patch free limit ($\bar{d} \to \infty$) of the natural logarithm of the evaporation time = 5.25.

FIG. 4. Comparison between mean evaporation time for regularly spaced and randomly placed hydrophilic patches of different sizes $L = 512$, $D = 10$. Dashed lines are guides to the eye.

L	patch size	l_s	$\bar{l}$	$\delta\bar{l}^2$
512	NA	NA	1.36	1.11
512	4	16	0.74	0.66
512	2	8	0.57	0.54
512	2	11	0.76	0.68
512	2	16	0.95	0.83

TABLE I. Mean vapor film thickness ($\bar{l}$) and mean square fluctuations ($\delta\bar{l}^2$) for regularly spaced patches. The film thickness is almost uniform over the entire walls, except at the sites where the attractive patches are located. This is *not* true if the patches are randomly distributed. In that case $\bar{l}$ decreases with the size of the patches and increases with center-to-center distance between the patches, l_s (i.e., increases with decreasing coverage).

D : L	32	64	128	512
6	160 (40) 0.3 ns			
7	220 (100) 1 ns			
8	330 (500) 7.5 ns	180 (60) 0.5 ns		
9	180 (9700) 80 ns	530 (200) 5 ns		
10		250 (2400) 27 ns	120 (350) 1.5 ns	60 (50) 0.15 ns

TABLE II. Comparison of mean tube formation times τ_{tube} from Glauber and Kawasaki dynamics, τ_G and τ_K, for different combinations of L and D. Three values are given. The first denotes the ratio τ_K/τ_G. The second (in brackets) gives τ_G, computed *after* equilibrating the vapor films with a no-breach constraint. The third number gives estimated tube formation times, τ_{tube}, in nanoseconds obtained from $\tau_K \times \Delta t$, where $\Delta t = 45fs$ is obtained by equilibrating diffusion constant for lattice gas, $D_{\text{lattice gas}} \sim 2.7x10^{-3}a^2/\text{pass}$ with diffusion constant for water, $D_{water} = 2.4x10^{-9}m^2/s$. Error bars are estimated at 10–20% of τ_K and are negligible for τ_G.

Θ (%)	1.25	2.5	5.0
	147 (77.5) 0.5 ns	167 (97.5) 0.75 ns	548 (800) 20 ns

TABLE III. Comparison of mean tube formation times for Glauber and Kawasaki dynamics, τ_G and τ_K, for a system $L = 512$, $D = 10$, at various hydrophilic coverage, Θ. The meaning of numbers is the same as in Table II.

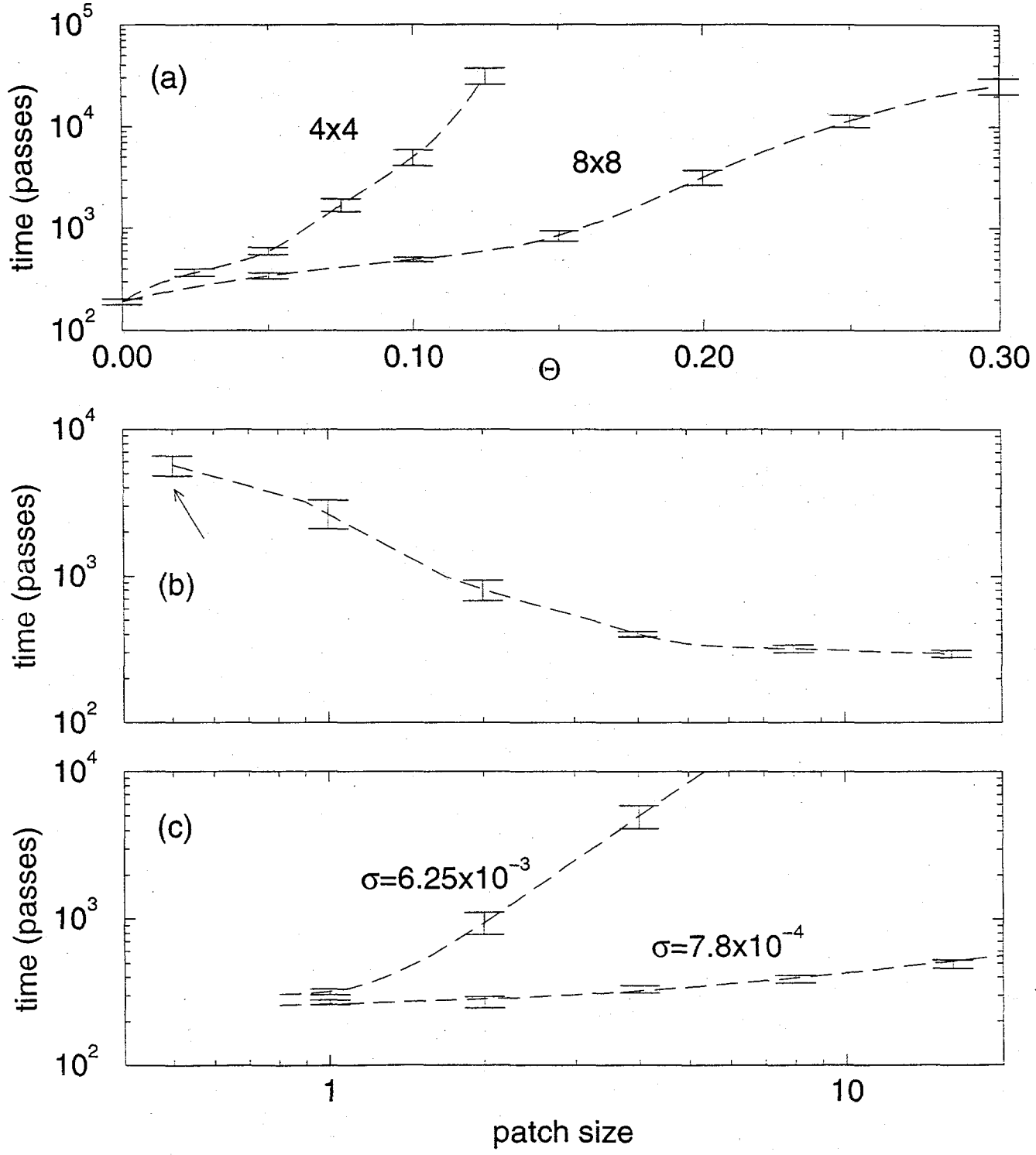

Luzar and Leung, Fig. 2

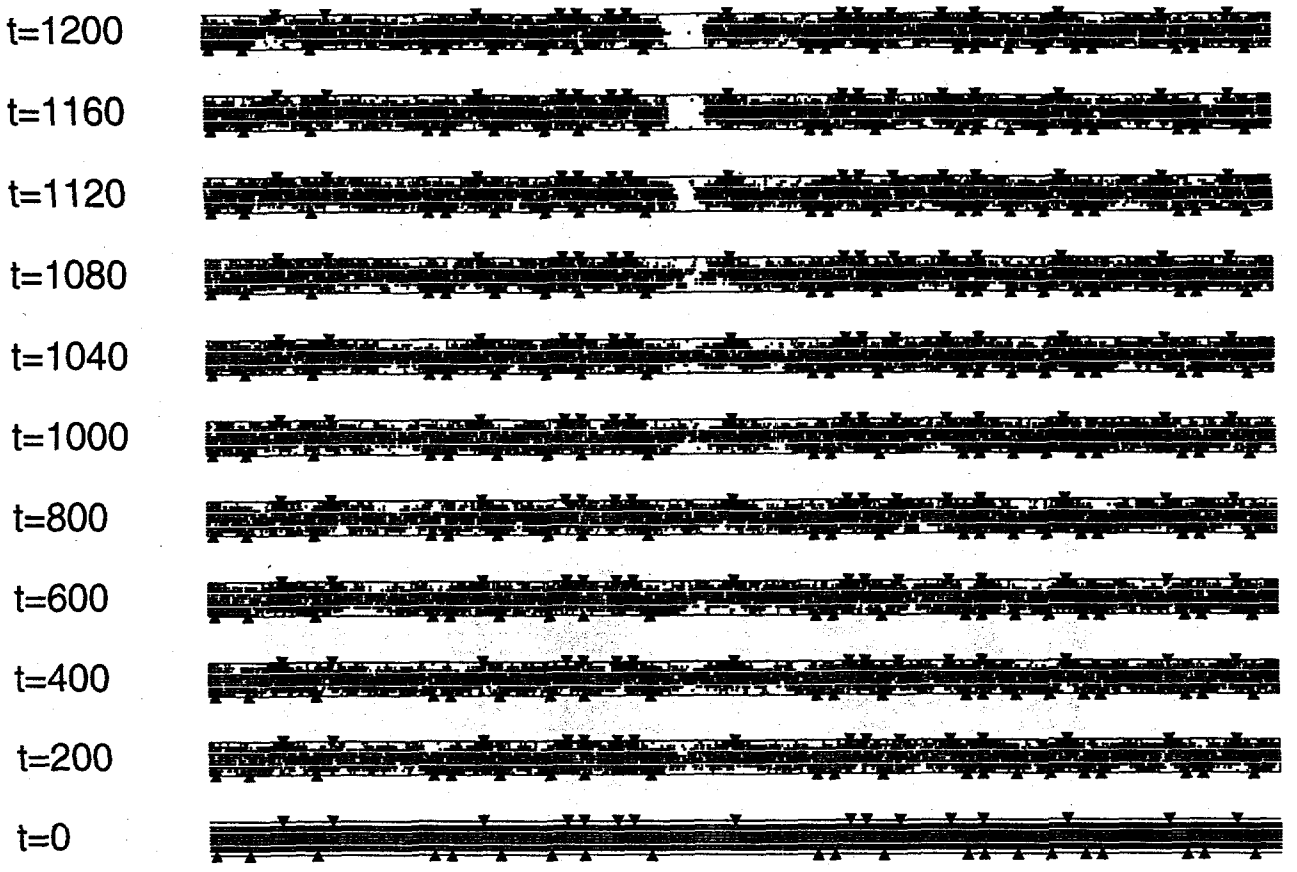

(a)

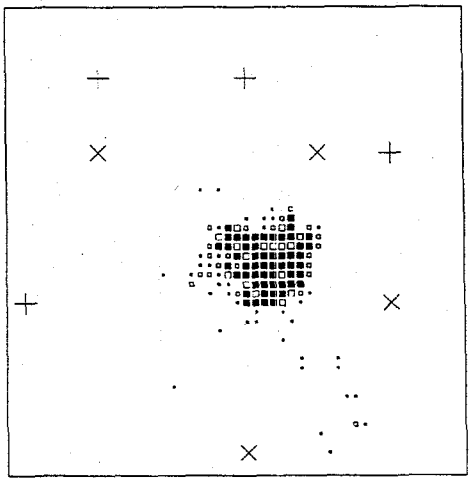

(b)

(c)

(d)

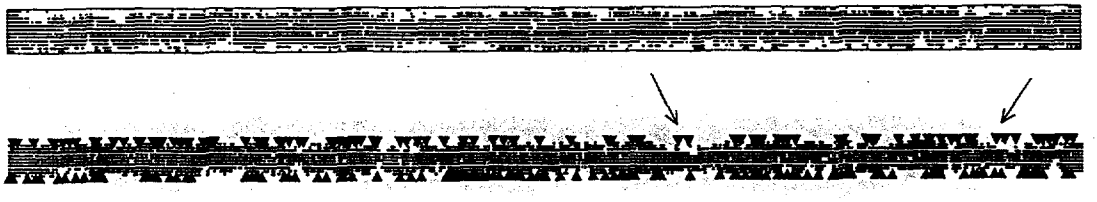

Luzar and Leung, Fig. 3

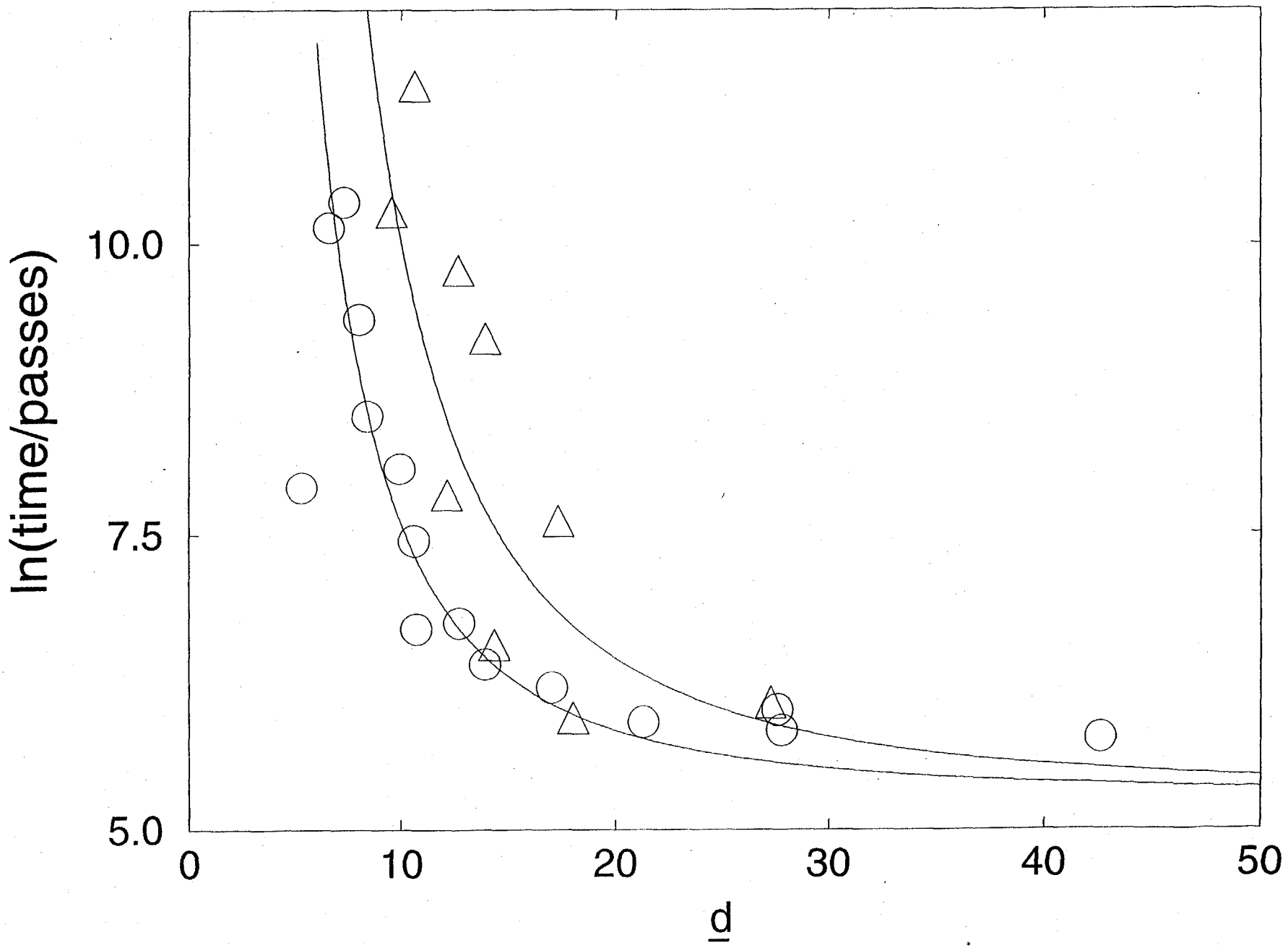

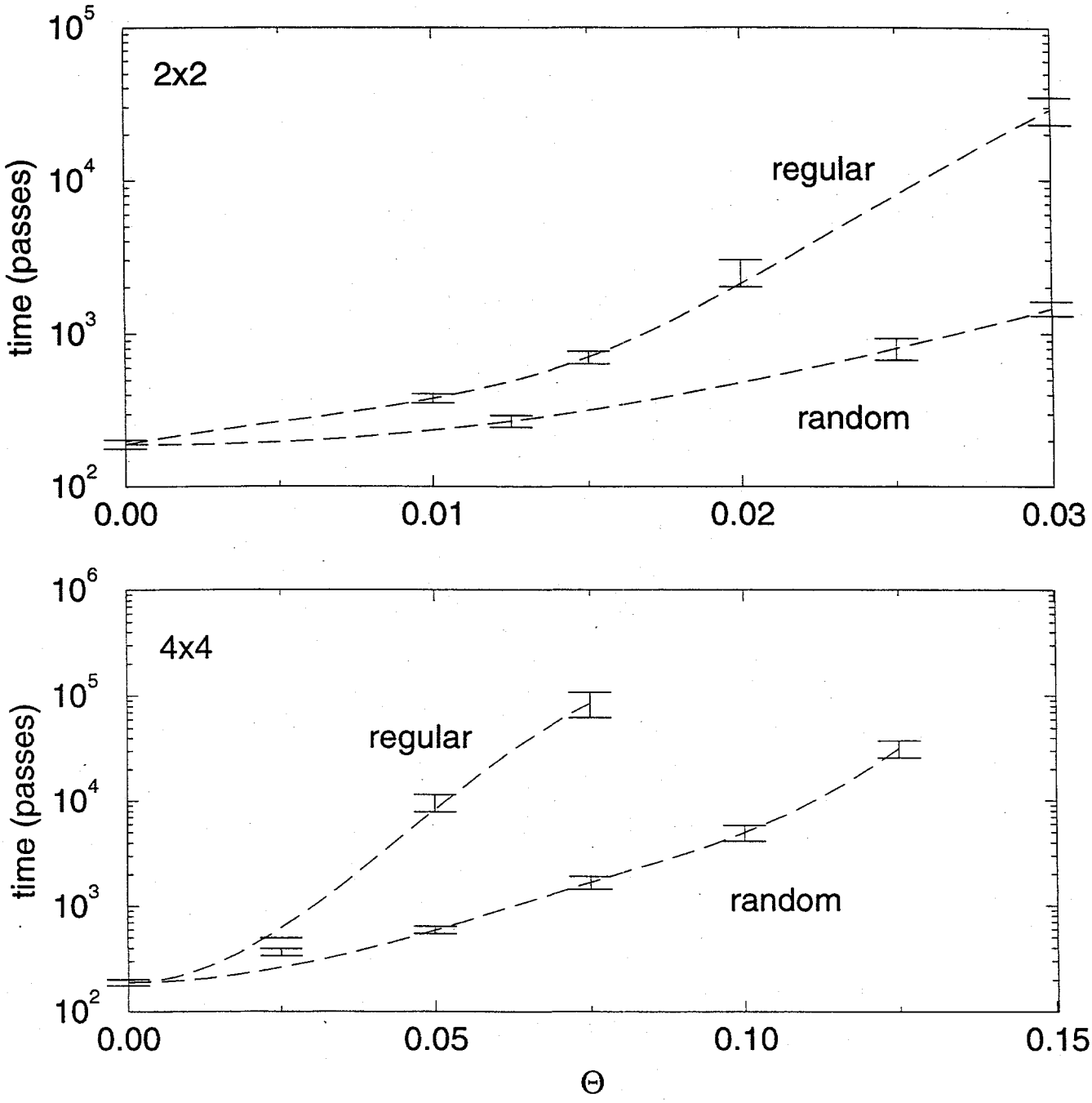

Luzar and Leung, Fig. 4